

Radio-Frequency Size Effect and the Fermi Surface of Tungsten

V. V. BOIKO AND V. A. GASPAROV

Sukhumi Physico-technical Institute, Institute of Solid State Physics, USSR Academy of Sciences

*Submitted July 15, 1971*Zh. Eksp. Teor. Fiz. **61**, 2362–2372 (December, 1972)

Anisotropy of the extreme dimensions of the tungsten Fermi surface in the two crystallographic planes (100) and (110) is studied by means of the radio-frequency size effect. The shape and size of all sections of both the electron and hole parts of the surface are determined on the basis of an analysis of the results obtained. An empirical model of the Fermi surface for tungsten is set up and compared with the Fermi surface for molybdenum and with the theoretical calculations. The differences are discussed from the standpoint of a possible effect of relativism on the band structure of the metals. Estimates are made of the electron and hole velocities in various sections of the Fermi surface of tungsten.

INTRODUCTION

TUNGSTEN is one of those few transition metals whose dynamic structure has by now been quite well investigated. During the last decade, the study of the electronic energy spectrum, and particularly the Fermi surface of this metal, has been the subject of a large number of both theoretical and experimental papers. The following were investigated experimentally: the anomalous skin effect^[1], the magnetoresistance^[2,4], magnetoacoustic^[5,6] and radio-frequency^[7-9] size effects, cyclotron resonance^[9-12], and the de Haas—van Alphen oscillations^[13-15]. The latest and most detailed paper is^[15]. Owing to the use of pulsed magnetic fields and computer reduction of the results, the authors of^[15] succeeded not only in obtaining detailed information concerning the anisotropy of the area of the extremal sections of all the divisions of the Fermi surface of tungsten, but also in determining its shape, dimensions, total surface area, and the volumes of the electronic and hole parts. Although the experimental data accumulated as a result of all these investigations are already quite appreciable, nonetheless their significance is adversely affected by the fact that the individual parameters of the Fermi surface of tungsten reported from different experiments are contradictory in character. This pertains in particular to the results of magnetoacoustic measurements and the de Haas—van Alphen effect.

Inasmuch as the observed disparity of the experimental data makes difficult a detailed quantitative comparison of the corresponding theoretical calculations of the band structure of tungsten^[16-20] with experiment, it was of interest to study the Fermi surface of this metal with the aid of one more method, which makes it possible to measure directly the linear dimensions of the electron orbits, namely the method of radio-frequency size effect (RSE). Such investigations were already performed in principle in^[7-9], but the information contained therein, first, pertains only to the (110) plane, and second, is limited to large sections of this surface.

By improving the experimental procedures and also the technology of preparing the samples necessary for these investigations, we obtained detailed data on all the sections of the Fermi surface of tungsten. The present paper is devoted to the results of the measurements and to their analysis.

EXPERIMENT

In the experiments we investigated the dependence of the surface impedance $Z = R + iX$ of single-crystal tungsten plates on the magnetic field H . At definite values of the magnetic field H_0 , the experimental dimensions of the electronic trajectories become equal to the plate thickness d , and this leads to the appearance of singularities on the dependence of the surface impedance on the magnetic field. The positions of these singularities with respect to the magnetic field make it possible to determine the corresponding dimension $2k$ of the electronic orbit in the wave-vector space:

$$2k = edH_0 / \hbar c. \quad (1)$$

The experimental setup and the investigation procedure were described in^[21,22]. In the experiments, we registered the first ($\partial R / \partial H$) and second ($\partial^2 R / \partial H^2$) derivatives of the active part of the surface impedance with respect to the magnetic field^[22]. The working frequency was 3.5 MHz, and the magnetic-field modulation frequency 18 Hz. The measurements were made at 1.5 and 4.2° K.

The samples were cut by the electric-spark method from single-crystal ingots of zone-purified tungsten of ~ 4 mm diameter with $R(300^\circ\text{K})/R(4.2^\circ\text{K}) \approx 3.5 \times 10^4$. The obtained disks were mechanically ground with M-10 silicon-carbide powder and then etched in a hot mixture of equal parts of HNO_3 , H_3PO_4 , and HF. The samples were oriented by x-ray diffraction with accuracy $\pm 30'$, and the thicknesses were measured with an IZV-2 vertical optimeter with accuracy $\pm 1 \mu$. The use of high-purity tungsten has made it possible to carry out investigations on samples ~ 0.3 mm thick. The error in the measurement of the sample thickness, connected with the fact that the samples were not plane-parallel, was $\pm 0.5\%$, and the error in the measurement of the line positions was ± 1.5 – 2.5% . As a result, the absolute values of the wave vectors were determined accurate to ± 2 – 3% .

The measurements were performed in a magnetic field parallel to the sample surface, with perpendicular polarization of the high-frequency electric and magnetic fields ($\mathbf{E} \perp \mathbf{H}$). To identify the sections, we used the dependence of the line position on the inclination of the magnetic field.

The anisotropy of the position of the RSE lines was

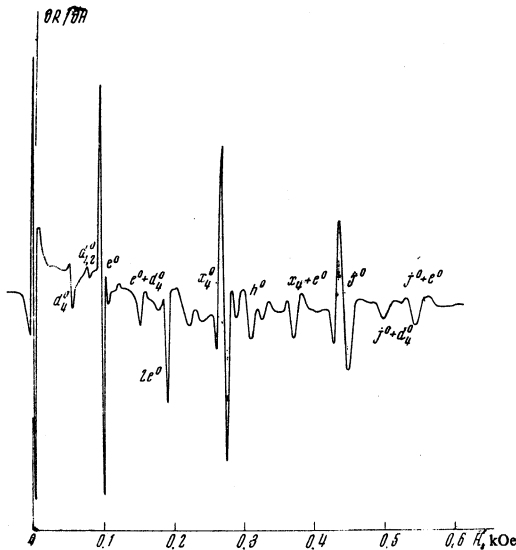


FIG. 1. Typical plot of size-effect lines for a sample with $n \parallel [100]$, $d = 0.340$ mm, $T = 4.2^\circ\text{K}$, $f = 3.5$ MHz, $H \parallel [001]$, and $E \perp H$.

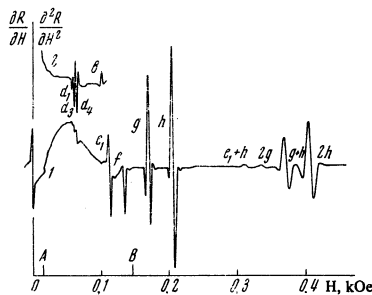


FIG. 2. Typical plot of size-effect lines for a sample with $n \parallel [110]$, $d = 0.336$ mm, $T = 4.2^\circ\text{K}$, $f = 3.5$ MHz, $H \parallel [121]$, $E \perp H$. Curves 1 and 2 are respectively plots of $\partial R/\partial H$ and $\partial^2 R/\partial H^2$. In section AB, the gain was increased by ten times for curve 1.

investigated on samples whose normals n to the surface coincided with the following crystallographic directions: $n \parallel [100]$ and $n \parallel [110]$. Typical plots of the RSE, observed in the (100) and (110) planes, are shown in Figs. 1 and 2. We see that in Fig. 2, the use of a plot of the second derivative ($\partial^2 R/\partial H^2$) has made it possible to resolve distinctly the closely-lying RSE lines. When the first derivative ($\partial R/\partial H$) is recorded, these lines are observed against the background of a strong nonmonotonic dependence of the surface impedance on the magnetic field.

The polar diagrams (Figs. 3 and 4) show the measured extremal dimensions of the sections of the Fermi surface of tungsten in the planes (100) and (110). The radii represent the quantity k , determined from formula (1), in units of k_0 , which is the limiting wave vector of the Brillouin zone in the [100] direction ($k_0 = 2\pi/a = 1.987 \text{ \AA}^{-1}$, $a = 3.162 \text{ \AA}$ is the lattice constant of tungsten at helium temperatures). The lines from the orbit chains are not shown in the diagram. The quantities corresponding to the (100) plane are marked with a zero superscript.

The field values used for the calculations were taken from the left edge of the line^[22]. The determination of the positions of these lines was simplified by the exis-

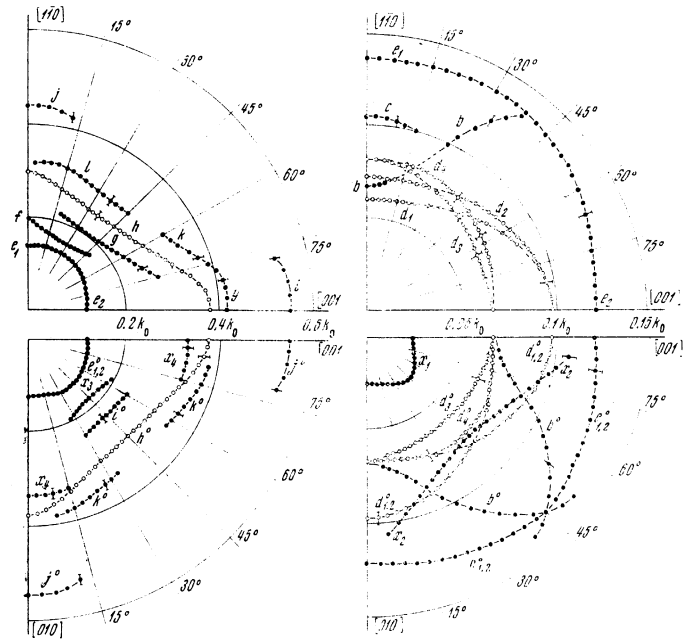


FIG. 3

FIG. 4

FIG. 3. Angular dependence of the half-width of the extremal orbits (in units of k_0) in the planes (110) and (100). The light and the dark circles denote the corresponding dependences for the electron and hole surfaces.

FIG. 4. Experimental results in the planes (110) and (100), pertaining to the small sections of the Fermi surface of tungsten. The notation is the same as in Fig. 3.

tence, in a zero field, of a narrow and intense line. This line was equally well observed for samples with different surface qualities, and its shape and intensity were independent of the orientation of the magnetic field relative to the crystallographic directions. Decreasing the sample thickness broadened the line, in analogy with the broadening of the RSE lines.

INTERPRETATION OF RSE LINES

A model of the Fermi surface of the chromium-group metals, proposed in^[16] and refined in^[17-19], is shown in Fig. 5. The electronic part of this surface is a "jack" with symmetry center at the point Γ of the Brillouin zone. It has a shape similar to an octahedron on whose corners are located convex spheroids. The intersections of the spheroids with the octahedron lead to the appearance of electronic lenses inside the necks of the jack. The hole surface consists of an octahedron at the point H with rounded edges and vertices, and six ellipsoids at the points N of the Brillouin zone.

A thorough analysis of the results shown in Figs. 3 and 4, using the procedure employed for the investigation of the RSE in molybdenum^[21,22], which has a similar Fermi surface, has shown that the observed RSE lines describe sufficiently well the majority of the sections of the theoretical model. Since we used the same letter designations for the RSE lines as in^[21,22], we shall describe the obtained results only briefly, dwelling in greater detail on those lines which were not observed in molybdenum.

The lines h and h^0 are due to the central cross sec-

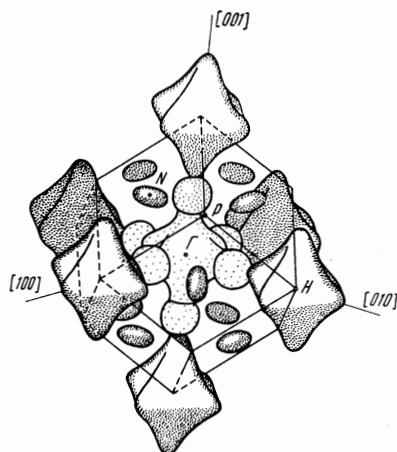


FIG. 5. Fermi surface of the metals of the chromium group.

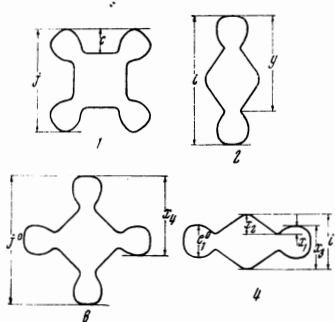


FIG. 6. Measured dimensions of the central sections of the electron surface: 1 and 2—plane (110), $H \parallel [001]$ and $H \parallel [\bar{1}10]$, respectively; 3 and 4—plane (100), $H \parallel [001]$ and $H \parallel [011]$, respectively.

tions of the hole octahedron. The lines of group d correspond to the orbits passing over the hole surfaces located at the points N of the Brillouin zone. As seen from Fig. 4, the angular dependence of the positions of these lines describes well the shadow projections of the ellipsoid.

The orbits passing through the central part of the electron jack correspond to the lines g, i, and j. Figure 6 illustrates the shape and measured dimensions of the

orbits. In addition to these lines, an entire series of lines are observed, which we connect with the following orbits: e—spheroids, b—necks of the electron jack, f—orbit passing through two necks and the octahedral part of the jack^[22]. The line y is due to the kink on the orbit i, which makes it possible to determine the distance from Γ to the plane of the neck. We did not succeed in observing the kink line due to the dimension from the end of the spheroid to the plane of the neck ($i - y$); this is apparently connected with the fact that the inequality $\Delta k/k \leq \Delta H/H$ was not satisfied for such an orbit (Δk is the curvature radius of the neck, k is the corresponding dimension of the electron orbit^[21], and $\Delta H/H$ is the relative width of the RSE line).

When the magnetic field is inclined away from the directions [110] and [001], lines l , k , and k^0 appear, which cannot be tied in satisfactorily with any orbit chains. They split with increasing inclination of the field, indicating that the corresponding sections are not central. As shown by an analysis of the model, such sections do indeed occur on the electron surface, and the orbits corresponding to them pass over the octahedral part of the jack and over either one (k , k^0) or two (l) spheroids. In the angle range $30^\circ \leq \varphi \leq 45^\circ$ (φ is the angle between H and [001]), the orbit l is due to the section with the extremal area—the “mouse” orbit^[20].

Owing to the complexity of the electron surface, the orbits passing over it have several effective points and this leads to the appearance of a number of RSE lines due to the emergence of the corresponding bursts on to the second surface of the sample. We attribute to these orbits the lines c , x_1 , x_2 , x_3 , and x_4 (Fig. 6). The line x_1 was observed by us only in the (100) plane, and therefore it cannot be connected with orbits on the electron lenses. Therefore the explanation given above for its origin seems to us to be the only one possible. From the anisotropy of the position of this line and of the line e^0 we can conclude that the intersection of the neck with the (100) plane is square.

Table I. Values of k-vectors of the Fermi surface of tungsten (\AA^{-1})

Measured dimension	Theory			Experiment					
	RSE	RSE	RAPW	Present work	APW	Magneto-acoustic effect		de Haas-van Alphen effect	
	[27]	[28]	[29]			[9]	[8]	[14]	[15]
Electron jack									
Γ_s	1.16	1.15	1.08	1.09 ± 0.02	1.11	1.04	1.18		1.098
Γ_g	0.47	0.44	0.36	0.41 ± 0.01	0.415		0.50		0.401
Γ_h	0.51	0.49	0.40	0.46 ± 0.01			0.51		0.475
Γ_Q				0.55 ± 0.01					0.554
Γ_O				—					0.888
O_p				0.27 ± 0.005			0.25	0.263	0.268
O_n				0.24 ± 0.005			0.24		0.24
Q_m				0.135 ± 0.004				0.136	0.132
Q_i				0.147 ± 0.004					0.147
Hole octahedron									
H_d	0.81	0.84	0.77	0.75 ± 0.015	0.78	0.70	0.78		0.760
H_f	0.50	0.53	0.49	0.50 ± 0.01	0.50		0.22		0.479
H_e	0.60	0.63	0.58	0.60 ± 0.01	0.60	0.59	0.23		0.584
Hole ellipsoids									
N_a			0.0	0.195 ± 0.006					0.195
N_b			0.0	0.143 ± 0.004					0.146
N_c			0.0	0.121 ± 0.004					0.125

Table II. Parameters of the Fermi surface of tungsten and molybdenum

Measured dimension	Theory				Experiment		
	Mo RSE [11]	WRSE [11]	WRAPW [19]	$k_{Mo} - k_W$	Mo APW [11, 21]	W APW [11, 21]	$k_{Mo} - k_W$
Electron jack							
Γs	1.15	1.15	1.08	0.07	1.16	1.09	0.07
Γg	0.44	0.44	0.36	0.08	0.47	0.41	0.05
Γh	0.49	0.49	0.40	0.09	0.52	0.46	0.06
ΓQ	—	—	—	—	0.57	0.55	0.02
$O p$	—	—	—	—	0.33	0.27	0.05
$O n$	—	—	—	—	0.29	0.24	0.05
$Q m$	—	—	—	—	0.18	0.135	0.045
$Q i$	—	—	—	—	0.18	0.147	0.033
Hole octahedron							
$H d$	0.84	0.84	0.77	0.07	0.79	0.75	0.04
$H f$	0.53	0.53	0.49	0.04	0.51	0.50	0.01
$H e$	0.63	0.63	0.58	0.05	0.60	0.60	0
Hole ellipsoids							
$N a$	0.368	—	0.0	0.368	0.37	0.195	0.18
$N b$	0.266	—	0.0	0.266	0.29	0.143	0.15
$N c$	0.189	—	0.0	0.189	0.22	0.121	0.10
$\Delta k = \Gamma H - (\Gamma s + H d)$			0.16		$0.05 \pm \pm 0.04$	$0.15 \pm \pm 0.04$	

*The k vectors are given in \AA^{-1} .

**Present results.

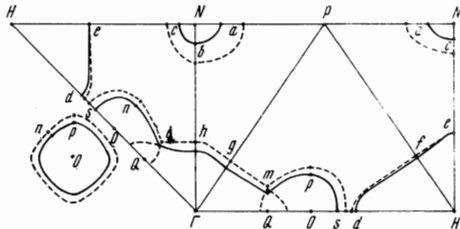


FIG. 7. Empirical model of the Fermi surface of tungsten (continuous curve) and of molybdenum (dashed curve).

DISCUSSION OF RESULTS

1. Empirical Model of Fermi Surface of Tungsten

Table I gives the main dimensions of the Fermi surface of tungsten, obtained on the basis of the performed investigations, together with the results of other experimental procedures and theoretical calculations. Figure 7 serves as an illustration of the measured dimensions.

As shown by Walsh and co-workers^[7-9] and confirmed by an investigation of the de Haas—van Alphen effect^[14,15], there is a gap between the hole octahedron and the electron jack. This gap is due to the splitting Δ_s of the degenerate states as a result of the spin-orbit interaction. We determined the gap at $\Delta k = 0.15 \pm 0.04 \text{ \AA}^{-1}$, which is 8% of the ΓH distance. The value 5% obtained by Walsh is connected with the fact that in the RSE investigations in^[7-9] the line positions were determined from the maximal extremum of the resonance, which exceeds the true value by an amount equal to the half-width of the line^[22]. Allowance for such a correction leads apparently to complete equality of these results.

As seen from Table I, the results are in good quantitative agreement with the model parameters determined from investigations of the de Haas—van Alphen effect. A certain difference, which slightly exceeds the measurement error, is apparently due to the fact that the

description in^[15] of the model of the Fermi surface of tungsten in the form of simple analytic functions is incomplete. It is possible that the faces of the electron jack and of the hole octahedron have depressions, as proposed in^[15]. However, since the RSE gives a shadow projection of the surface on the plane of the intersection, we were unable to reconstruct the shapes of these faces. Even if these depressions do occur, their magnitude does not exceed the measurement error, for otherwise the dimensions of the electron and hole surfaces along [111] (Γg and $H f$), determined from the RSE investigations, would be larger than the results obtained in^[15].

The information obtained from investigations of the magnetoacoustic effect^[5,6] is somewhat contradictory (see Table I), which makes a direct comparison with the results of the present communication difficult. Such a situation is apparently connected with the fact that the results in^[5,6] were obtained during the earlier stage of the investigations, when there were no detailed theoretical calculations of the model of the Fermi surface of tungsten.

A comparison of the empirical model with the theoretical one^[20], obtained from a relativistic calculation of the band structure of tungsten by the method of augmented plane waves (RAPW) shows them to be in good albeit insufficiently complete agreement. In particular, the hole ellipsoids N, the existence of which has been experimentally demonstrated, are missing in the relativistic model.

2. FERMI SURFACE OF TUNGSTEN AND MOLYBDENUM

Molybdenum and tungsten are elements of the sixth group of the periodic table, the chromium group. In the theoretical calculations of the band structure of these metals, the atomic configurations of the valence electron shells are assumed to be $(4d)^5(5s)^1$ and $(5d)^5(6s)^1$ for molybdenum and tungsten, respectively. Both elements crystallize into a body-centered cubic lattice with

helium-temperature parameters $a = 3.143 \text{ \AA}$ (for molybdenum) and $a = 3.162 \text{ \AA}$ (for tungsten). Calculations of the band structures of these metals have been the subject of several communications^[17-20]. The calculations were performed by the augmented plane wave (APW) method in both the nonrelativistic approximation^[17,19] and with allowance for the relativistic correction^[18,20].

Louck's nonrelativistic calculation results in complete agreement between the Fermi surfaces of these metals^[19]. At the same time, allowance for the relativistic effect^[20] shows that whereas in molybdenum ($Z = 42$, where Z is the atomic number) they are negligibly small, in tungsten ($Z = 74$) the relativistic corrections leads to significant changes in the Fermi surface.

In the relativistic model, an overall decrease of the surface dimensions is observed. The spin-orbit interaction leads to the appearance of a gap between the hole octahedron and the electron jack and to a vanishing of the electron lenses. The relativistic calculation did not reveal the presence of hole ellipsoids in N in the model.

In addition, Mattheis^[17], using for the calculations two values of the potential that differ by 30% in the contribution of the exchange terms, observed that the model of the Fermi surface of tungsten is sensitive to changes of this type. It would therefore be natural to compare the Fermi surfaces of these two metals on the basis of data obtained by using identical approximations.

The results of such a comparison, together with the data obtained from the RSE measurement^[21,22], are given in Table II and in Fig. 7. As seen from the results, the contribution of the relativistic effects turns out to be appreciable not only for tungsten, but also for molybdenum. Although these corrections are much smaller for molybdenum (see Table II), nevertheless the spin-orbit interaction in molybdenum has led to the existence of gaps between the hole octahedron and the electron jack and between the neck and the lens.

A comparison of the experimental results for tungsten confirms the overall decrease of the Fermi surface predicted in the relativistic model. The theoretical value of the gap is in good agreement with the experimental one. The vanishing of the electron lenses, due to spin-orbit interaction, has been confirmed.

At the same time, the existence of hole ellipsoids in N has been experimentally proved. The vanishing of this surface in the theory is connected not with the spin-orbit interaction but with the relativistic corrections in the effective potential, to the form of which the states N'_1 , which are responsible for the occurrence of the ellipsoids, are highly sensitive. It is probable that the obtained experimental information will make it possible to refine the form of the potential.

Investigations of the optical properties of tungsten and molybdenum have shown that there are maxima of absorption at $h\nu \sim 1.0 \text{ eV}$ for tungsten^[24,25] and $h\nu \sim 0.4 \text{ eV}$ for molybdenum^[26]. These singularities are connected in^[27] with the threshold of the quantum transitions between the $\Delta_6 - \Delta_7$ states, which arise as a result of the spin-orbit splitting of the Δ_5 states in the band structure of these metals. Using these results and the values of the gap given in Table II, we can estimate the velocities of the electrons and of the holes at the limiting points of the electron jack and of the hole octahedron along the ΓH axis, using the formula

$$v = \Delta E / \hbar \Delta k, \quad (2)$$

where ΔE is the energy splitting and $\hbar \Delta k$ the momentum splitting. The estimate yields a value $v_{M_0} \approx v_W \approx 1 \times 10^8 \text{ cm/sec}$, which is correct in order of magnitude.

Using the empirical model of the Fermi surface of tungsten and the values of the effective masses of the carriers on the central parts of the Fermi surface from^[9,11], we have determined the average velocities of the electrons and holes on the central intersections of the electron jack and of the hole octahedron by the (111) plane, using the formula^[21]

$$\bar{v} = \frac{\hbar k}{2\pi m^*} |\cos 19^\circ 18'|^{-1}, \quad (3)$$

where $\hbar k$ is the length of the orbit in momentum space, and m^* is the cyclotron effective mass. The values obtained turned out to be

$$\bar{v}_e = 0.67 \cdot 10^8 \text{ cm/sec}, \quad \bar{v}_h = 1.23 \cdot 10^8 \text{ cm/sec}.$$

The analogous values obtained for molybdenum^[21] were

$$\bar{v}_e = 0.60 \cdot 10^8 \text{ cm/sec}, \quad \bar{v}_h = 0.89 \cdot 10^8 \text{ cm/sec}.$$

The complicated character of the Fermi surfaces of tungsten and molybdenum leads to the existence of a large number of carriers with close and small values of the effective masses, which makes their interpretation difficult. Nevertheless, Walsh^[9] succeeded in identifying the previously obtained results by investigating the cyclotron resonance in tungsten and in tying in the orbit passing through the central section of the hole ellipsoid by the (100) plane with a value 0.23 for the cyclotron effective mass. The corresponding value obtained from the temperature dependence of the amplitude of the oscillations of the de Haas—van Alphen effect is 0.28. The average carrier velocity on the hole ellipsoids, estimated from the obtained values using formula (3) (without the cosine), turned out to be $\bar{v}_h \approx 0.6 \times 10^8 \text{ cm/sec}$.

The absence of suitable information for molybdenum did not make it possible to make an analogous estimate. Nonetheless, the obtained values of the velocities offer evidence, apparently, that there are no carriers with significantly differing velocities on the Fermi surfaces of molybdenum and tungsten.

In conclusion, the authors consider it their pleasant duty to thank V. F. Gantmakher for a detailed discussion of the results and for valuable advice, M. I. Kaganov for interest in the work, and G. N. Landysheva for help with the measurements.

¹E. Fawcett and D. Griffiths, *J. Phys. Chem. Solids* **23**, 1631 (1962).

²E. Fawcett, *Phys. Rev.* **128**, 154 (1962).

³E. Fawcett and W. A. Reed, *Phys. Rev. A* (1964-1965) **134**, 723 (1964).

⁴N. V. Vol'kenshtein, V. A. Novoselov, and V. A. Startsev, *Fiz. Metal. Metalloved.* **22**, 175 (1966).

⁵J. A. Rayne, *Phys. Rev. A* (1964-1965) **133**, 1104 (1964).

⁶C. K. Jones and J. A. Rayne, *Proc. IX Intern. Conf. on Low Temp. Phys.*, Plenum Press, N.Y., 1965, p. 790.

⁷W. M. Walsh, Jr. and C. C. Grimes, *Phys. Rev. Lett.* **13**, 523 (1964).

⁸W. M. Walsh, Jr., C. C. Grimes, G. Adams, and L. W. Rupp, *Proc. IX Intern. Conf. on Low Temp. Phys.*, Plenum Press, N.Y., 1965, p. 769.

⁹W. M. Walsh, *Resonances both Temporal and Spatial* (lectures given at the Simon Fraser Summer School of Solid State Physics), 1967.

¹⁰E. Fawcett and W. M. Walsh, Jr., *Phys. Rev. Lett.* **8**, 476 (1962).

- ¹¹W. M. Walsh, Jr., Phys. Rev. Lett. **12**, 161 (1964).
- ¹²R. Germann and V. S. Édel'man, Zh. Eksp. Teor. Fiz. **53**, 1563 (1967) [Sov. Phys. JETP **26**, 901 (1968)].
- ¹³G. B. Brandt and J. A. Rayne, Phys. Rev. **132**, 1945 (1963).
- ¹⁴D. M. Sparlin and J. A. Marcus, Phys. Rev. **144**, 484 (1966).
- ¹⁵R. D. Girvan, A. V. Gold, and R. A. Phillips, J. Phys. Chem. Solids **29**, 1485 (1968).
- ¹⁶W. M. Lomer, Proc. Phys. Soc. Lond. **80**, 489 (1962); Proc. Phys. Soc. Lond. **84**, 327 (1964).
- ¹⁷L. F. Mattheiss, Phys. Rev. A (1964-1965) **139**, (6), 1896 (1965).
- ¹⁸L. F. Mattheiss and R. E. Watson, Phys. Rev. Lett. **13**, 576 (1964).
- ¹⁹T. L. Loucks, Phys. Rev. A (1964-1965) **139**, 1181 (1965).
- ²⁰T. L. Loucks, Phys. Rev. **143**, 506 (1966).
- ²¹V. V. Boiko, V. A. Gasparov, and I. G. Gverdtsiteli, Zh. Eksp. Teor. Fiz. **56**, 489 (1969) [Sov. Phys. JETP **29**, 267 (1969)].
- ²²V. V. Boiko and V. A. Gasparov, Zh. Eksp. Teor. Fiz. **61**, 1976 (1971) [Sov. Phys. JETP **34**, (1972)].
- ²³V. F. Gantmakher and I. P. Krylov, Zh. Eksp. Teor. Fiz. **47**, 2111 (1964) [Sov. Phys. JETP **20**, 1418 (1965)].
- ²⁴A. P. Lenham, J. Opt. Soc. Amer. **57**, 473 (1967).
- ²⁵S. Roberts, Phys. Rev. **114**, 104 (1959).
- ²⁶M. M. Kirillova, G. A. Bolotin, and V. M. Maevskii, Fiz. Metal. Metalloved. **24**, 95 (1967).
- ²⁷Yu. P. Udoev, N. S. Koz'yakova, and M. L. Kapitza, Fiz. Metal. Metalloved. **31**, 439 (1971).

Translated by J. G. Adashko
249